Experimental analysis of atmospheric heat sinks as heat dissipators

MCarmen Guerrero Delgado[a*], José Sánchez Ramos[b], MCarmen Pavón Moreno[a], José Antonio Tenorio Ríos[c], Servando Álvarez Domínguez[a]

[a] Grupo de Termotecnia, Escuela Superior de Ingenieros, Universidad de Sevilla, Camino de los Descubrimientos s/n. 41092, Seville, Spain.

[b] Máquinas y Motores Térmicos, Escuela Superior de Ingeniería, Av. Universidad de Cádiz, 10, 11519, Puerto Real, Spain

[c] Instituto de Ciencias de la Construcción Eduardo Torroja – CSIC, Serrano Galvache 4, 28033 Madrid, Spain.

**Corresponding author. mail address: mgdelgado@us.es (MCarmen Guerrero Delgado)*

Abstract

Overheating, a general problem both in urban spaces and inside buildings, calls for the deployment of passive cooling techniques to reduce energy consumption, protect the environment and institute satisfactory comfort levels. A key factor in such techniques is the capitalisation on the cooling potential of natural heat sinks. The sky, one such sink, has essentially limitless cooling power. In addition, its temperature on fair nights is lower than that of other environmental sinks (ground and air). The sky's promise in that respect prompted this exploration of the potential of nocturnal radiation cooling. A review of the state of the art revealed that in all the radiative dissipators developed and tested to date the dissipation fluid (water) transferred heat indirectly to the heat sink (the sky) by circulating water inside solar collector pipes. The highest values reported for maximum dissipation power were on the order of 100 W/m^2. The present study aimed to asses night time dissipation power in a dual system in which water circulated either inside pipes or flowed down the outer surface of the collector. The two modes, one involving in-pipe circulation and the other outer surface downflow, were compared experimentally, for whereas the former has been analysed and assessed by earlier researchers, the latter has not. The empirical findings verified that downflow setups enhanced cooling, delivering up to five-fold the dissipation power obtained with the conventional arrangement.

Keywords: overheating; passive cooling; radiative cooling; natural sinks; heat dissipation

1 Introduction

Context

Global and local climate change, in conjunction with projected population growth and economic development, have induced a general problem of overheating in both urban areas and building interiors [1], [2]. The energy demand for cooling is expected to rise steeply, eventually becoming the predominant component in that demand [3]. Such predictions determine a need to develop passive cooling techniques to lower energy consumption and protect the environment while ensuring satisfactory comfort levels.

Heat sinks

Buildings and urban areas exchange energy naturally with their surrounds. The elements involved in that natural mechanism are the sky, air, water and ground, all of which act as sinks. Energy-conscious design seeks to harness the natural resources located in the proximity of the building or urban area to be conditioned: solar energy, wind, ambient temperature, humidity, water and plant life. Natural cooling strategies consist of passive conditioning techniques to maintain comfort levels without consuming energy [4].

The techniques to lower indoor temperatures with passive conditioning techniques can be differentiated depending on whether water or air is used as the dissipation fluid. Air is used in natural ventilation (wind [5] and buoyancy [6] -driven ventilation, Trombe walls [7], [8] and solar chimneys [9], [10]), ventilation air pre-cooling (with the ground or sky as natural sinks [11], [12]) and heat dissipation with pre-cooled air (in thermally activated building systems, TABS [11], [13]) or other innovative building envelope applications. The higher specific heat in water than in air makes the former particularly promising, for it can carry large amounts of heat at a reasonably low flow rate. Given its better performance as a heat transfer fluid, water was chosen as the dissipation fluid for this study.

Water is used as a dissipation fluid in systems where heat is released across conventional elements such as fan coils or radiators as well as in innovative approaches such as thermally activated building systems (TABS)[13]. The latter use phase change materials (PCMs) as an alternative to increasing the thermal inertia of thermal storage elements in more conventional schemes [14]–[17].

Such systems operate with cold water, the source of which may be the ground as a natural sink [18], evaporative cooling [19]–[22] or nocturnal radiation cooling [23]–[28]. The ground, an eco-friendly and highly efficient heat dissipator, has been widely used for such purposes. At depths of approximately 2.5 m to 3 m, the ground temperature is known to be cool and constant year-round [29], although not as low as in the other sinks (wet-bulb air and sky temperatures). The ground may also become heat-saturated, posing efficacy problems [30]. Evaporative cooling has gained in popularity in recent years for its simplicity, low cost and use of renewable resources [4]. Its high cooling efficiency makes it an attractive alternative to conventional systems in warm, dry climates. Evaporative water loss is a drawback, however, against a backdrop of the constant universal growth of water consumption [31]. Cooling power may also be limited by air saturation, lowering the efficacy of that natural sink. The sky is a more effective sink than the other two systems. As a resource, it is unlimited, for it is always cold enough to dissipate heat. In addition, since on cloudless nights, the temperature is lower in the sky than in the ground or air (wet-bulb) [32], this study on nocturnal radiation cooling focused on its potential as a natural sink.

Nocturnal radiation cooling

Nocturnal radiation cooling systems aim to cool the water used as a conditioning fluid directly by circulating it through a radiation panel. The theoretical and empirical studies conducted on the use of radiation panels in nocturnal radiation cooling can be classified by radiation panel properties and setup. Ali et al. [33] experimented with a radiation system consisting of two vertically parallel panels through which water circulated, the top made of black-painted aluminium covered with polyethylene film. The maximum dissipation power attained was 54 W/m^2 at a flow of 17 kg/h, which lowered the water temperature by around 3 °C. Eicker et al. [34] developed a hybrid photovoltaic-thermal (PVT) system to generate electricity during the day and cold water for cooling at night. The water circulated inside the pipes located within the panel. The mean cooling power reached was 41 W/m^2 in the climate conditions prevailing in central Spain with ceiling ranged from 21 °C at start-up to 15 °C in the early morning. Xu et al. [35] analysed and tested a nocturnal radiation system with flat panel solar collectors in Beijing. In their system water cooled by convection and radiation into the sky at night was circulated through a 2 m^2 flat panel radiation collector. When tested from 18:00 to 07:00, the system lowered the water temperature from an approximate 24 °C at the outset by 4 °C. In the summer of 2014 Pean et al. [36] experimented with a PVT system at the University of Denmark. The mean cooling power ranged from 20 W/m^2 to 75 W/m^2 and the energy dissipated throughout the night from 0.2 kW/hm^2 to 0.9 kW/hm^2, depending on weather conditions. Hu et al. [37] proposed a dual-purpose collector to deliver heat during the day and cooling energy at night. Their hybrid photo-

thermal cooling and radiating collector was coated with black acrylic paint. A photo-thermal radiation prototype was manufactured and experimentally studied in both heating and cooling modes, with the water circulating inside the system pipes. The net radiation cooling flow attained with a clear night time sky was 55.1 W/m^2. The photo-thermal radiation nocturnal cooling energy gain was 0.99 MJ for 11.5 consecutive hours with a 3.9 °K decline in water temperature. Hu et al. [38] also developed a hybrid PV-T-RC system able to generate electric power and heat during the day and cooling energy at night. The maximum empirical cooling in a clear night time sky was observed to be 72 W/m^2. During nocturnal operation with clear skies the total PV-PT-RC system cooling energy gain was 2.90 MJ. Zhang et al. [39] developed a metamaterial hybrid made of a silver-plated glass fibre polymer to deliver higher cooling power, for which they reported a daily mean of 100 W/m^2. Bin Zhao et al. propusieron una estrategia novedosa para la construcción de sistemas fotovoltaicos integrados y sistemas de enfriamiento radiativo (RC), a saber, el sistema BIPV-RC, cubriendo el lado soleado de una azotea con módulos fotovoltaicos y su lado libre con módulos RC de todo el día para integrar la energía solar. recolección y utilización de RC en una sola unidad de construcción. Los resultados indican que la producción total de energía anual del sistema BIPV-RC es casi 79.1% y 16.8% más alto que el del sistema BIPV y BIRC, respectivamente [40]Ablimit Aili et al. desarrollaron gracias al avance de los materiales de enfriamiento radiative, un sistema de enfriamiento cuyo sumidero de calor es el cielo con una operación continua de 24h. Estos lograron potencias de enfriamiento promedio de 80 W/m2 durante el día y 100 W/m2 durante la noche [41]. Junwei Liu et al. [42]estudiaron un modulo de regulación de temperaturas para el enfriamiento directo en verano y el calentamiento en invierno. El modelo desarollado por dichos autores revela importantes ahorros de electricidad dado la no necesidad del sistema de acondicionamiento convencional. Dichos ahorros llegan a estimarse en el 63% al acoplar el sistema a un sistema de almacenamiento.

The conclusion drawn from the aforementioned studies and the review papers [43]–[45] consulted was that in all the radiation dissipators developed and tested the dissipation fluid (water) transferred heat indirectly to the heat sink (the sky), in most setups by circulating water inside collector pipes. The maximum dissipation power observed by these authors was on the order of 100 W/m^2.

Aims and originality

Given that, as noted throughout this introduction, the sky is a natural heat sink with high cooling potential, the object of the research conducted here was nocturnal radiation cooling. A review of the state of the art revealed that in all the radiative dissipator systems developed and tested to date the dissipation fluid (water) transferred heat indirectly to the heat sink (the sky) with maximum cooling power on the order of 100 W/m^2. This article presents an innovative dissipation system based on convective-radiant-evaporative transfer designed specifically for that purpose. Whilst nocturnal dissipation with water circulating inside pipes has been assessed and contrasted by earlier authors, none has addressed a system in which the water flows down the upper surface of the collector (downflow). Nocturnal dissipation based on water flowing outside the collector foreseeably raises cooling power because the heat carried by the water is transferred directly to the cold source. In addition, given the direct water-air contact in such arrangements, the cooling mechanism is evaporative, which favours heat dissipation. The aim sought in this study was consequently to experimentally assess the nocturnal dissipation power of a system in which water flowed down the upper surface of the collector (downflow) and compare its cooling power to that of conventional systems in which the water circulates inside radiating panel pipes.

2 Description of the collector and experimental setup

Collector

The radiator used in the experiment, marketed under the tradename ‘Solapool’, is deployed primarily to heat swimming pool water in mild climates. This 2 m long, 1.2 m wide unit consists of very thin (6 mm outer ϕ, 4.5 mm inner ϕ) polypropylene pipes. Although initially designed to heat water, given its finless, small diameter pipes, the ‘Solapool’ collector is apt for use in radiation cooling. Polypropylene is the material of choice for nocturnal radiation cooling, for it is characterised by low reflectivity and transmittance in the atmospheric window, which is tantamount to high emissivity (approximately 0.95) [45]. Such collectors are, moreover, highly price-competitive.

Experimental facility

The experimental prototype was positioned on the roof of the Seville School of Engineering in an area where the surrounds barely impacted the exchange between panel and sky.

The radiation cooling system tested comprised the polypropylene collector described and a 200 L storage tank containing the water to be cooled. The collector rested on a 9 cm thick layer of insulation to prevent heat transfer from below, whilst the entire body of the storage tank was wrapped in 6 cm thick insulation to minimise thermal loss.

As noted, the experiment aimed to assess and compare panel operation in:

- Operating mode 1: water circulating inside pipes (in-pipe)
- Operating mode 2: water flowing down the collector surface (downflow).

The setup was consequently designed with two separate circuits and the collector itself installed on a slant (Figure 1).

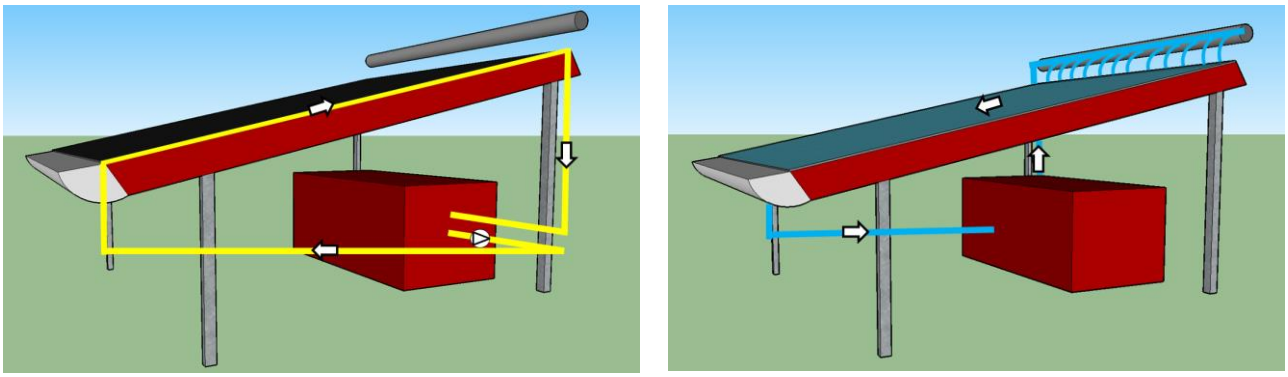

Figure 1. Nocturnal cooling system: left, operating mode 1; right, operating mode 2

In the operating mode 1 circuit (yellow line in Figure 1, left) the pump drove the water inside the pipes in the direction shown. In the mode 2 circuit (blue lines in Figure 1, right), water was pumped from the tank to a linearly perforated PVC pipe located above the high end of the collector. From there it streamed through the holes, forming a thin film that flowed across the collector and emptied into a PVC gutter at the low end, connected to the tank. As the gutter was at a higher elevation, the return water was gravity-driven back to the deposit with no need for pumping.

Monitoring system

The monitoring system was designed to gather data on the variables used to assess system operation and energy consumption: tank water temperature and temperature T the thermal balance between the collector and the outdoor weather conditions (dry- and wet- bulb outdoor air temperature and relative humidity).

2.3.1 Tank water temperature

The temperature of the tank water to be cooled was monitored with type T thermocouples operating in a range of -200 °C to +260 °C with a precision of ±0.1 °C. Consisting in one copper and one copper-nickel (55 %-45 %) alloy wire, these sensors were calibrated in a Fluke Calibration 9142 metrology well designed to cool to -25 °C and heat to +660 °C with a precision of ±0.01 °C. As the photograph and diagram in Figure 2 shows, thermocouples 1 to 5, which measured water temperature directly, were located at different points and heights in the tank, whilst thermocouples 6 and 7 were positioned in the thermal wells.

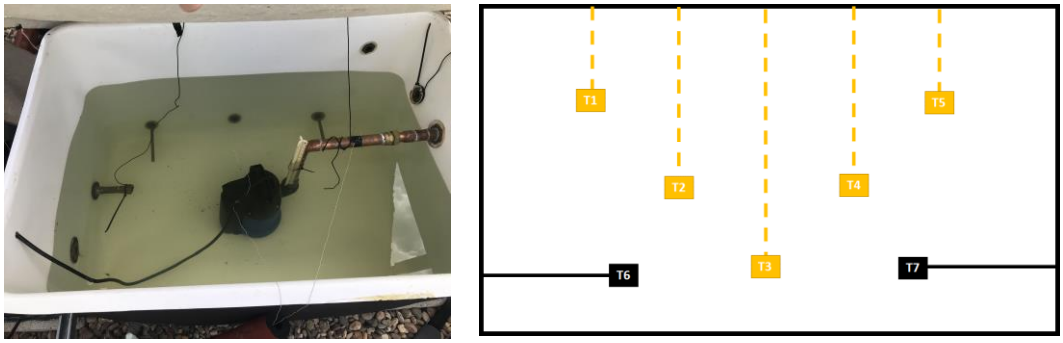

Figure 2. Thermocouple positions inside the water tank

2.3.2 Collector equilibrium temperature

The overnight outdoor air and sky temperatures acted as stimuli for the radiation cooling system, generating the heat flows depicted in Figure 3: convection-driven between the top surface of the collector and the air and heat transfer-driven due to longwave radiation between the top of the collector and the sky and surrounds. Given the 9 cm thick insulation under the bottom of the collector, conduction heat transfer between the roof and collector was deemed negligible.

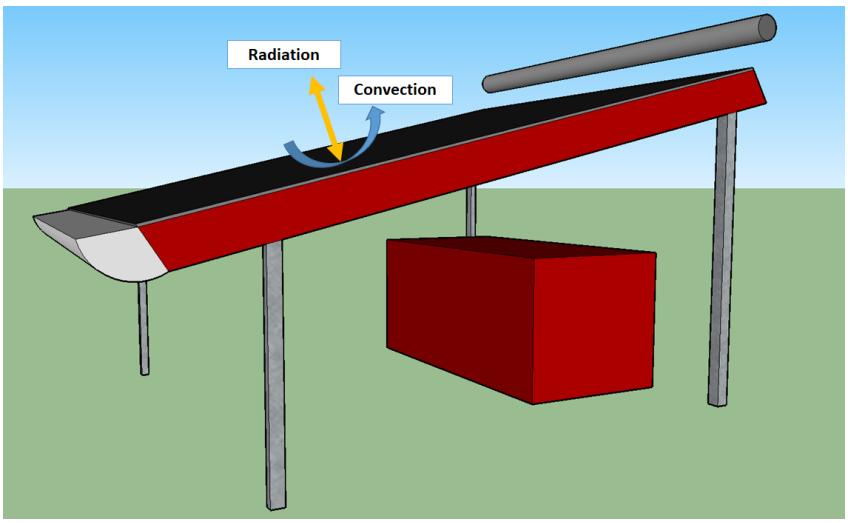

Figure 3. Heat transfer flows in the radiation panel

Equilibrium on the outer top surface of the collector would be found with Equation 1:

$$0 = F_{surface-sky} \cdot \sigma \cdot \varepsilon \cdot \left(T_{surface}^4 - T_{sky}^4\right) + F_{surface-surrounds} \cdot \sigma \cdot \varepsilon \cdot \left(T_{surface}^4 - T_{surrounds}^4\right) + h \cdot \left(T_{surface} - T_{air}\right)$$ (Eq.1)

The collector surface temperature recorded ($T_{surface}$) was the equilibrium T in the presence of the stimuli depicted in Figure 3 and the absence of circulation water. That value, the temperature equivalent to conduction and radiation heat transfer, here denominated equivalent temperature (T_{eq}), identified a cold source in the radiation system.

Likewise, the equivalent heat transfer temperature (T_{eq}) is the minimum temperature that the water would reach under certain climatic conditions. The time or area required to reach this temperature depends on the water inlet temperature and its flow rate. [46]

T_{eq} was measured with a prototype equivalent to the radiation system located alongside the collector (Figure 4, left). The prototype, a 12.4x10.6 cm replica of the collector, was lined at the bottom with 9 cm of insulation. Three type T thermocouples secured to the bottom of the prototype with a high thermal conductivity element measured the surface (equivalent) temperatures.

Figure 4. Equilibrium temperature measurement

2.3.3 Outdoor climate conditions

The outdoor climate conditions were recorded with a weather station and a sky meter located at a short distance from the prototype [47] (Figure 5). The weather station took outdoor air temperature, wind speed and relative humidity readings at 1 min intervals with a precision of ±0.1 % for temperature and wind speed and ±1 % for relative humidity. The sky meter recorded cloudiness at 15 seconds intervals.

Figure 5. Meteo station and sky meter [48]

In addition, dry outdoor air thermometers and relative humidity sensors were installed in situ to verify and duplicate the measurements. The thermocouple positioned as shown in Figure 6 measured dry outdoor air temperature. The metering face of the thermocouple was set in an insulated pipe fitted with a fan at one end to induce forced convection and prevent undesired measuring errors due to solar radiation, stagnated air or similar.

Figure 6. In situ measurement of outdoor air temperature

Relative humidity readings were also taken with three EasyLog dataloggers at different points in the system as shown in Figure 7, which recorded the relative humidity with a precision of ±0.5 %.

Figure 7. In situ relative humidity measurements

2.3.4 Data collection and control software (Labview)

Two National Instruments modules (NI TB-9214 and NI Cdaq-9174) were used to convert the differences in thermocouple power readings to temperature, whilst experimental system operation was controlled with Labview engineering software [49]. The thermocouples positioned on the tank for duplicate outdoor air and equivalent temperatures took readings at 1 min intervals, 24/7. System operating times, experiment modes and start-up and shutdown temperatures were programmed with Labview software.

3 System assessment methodology

[redacted]Aim

The methodology deployed to meet the aim (see sub-section 1.4) of the study is described hereunder.

Whilst the cooling power of in-pipe systems is characterised by two cold sources, air and sky, heat transfer efficacy is affected adversely by the convective resistance of the circulating water and the conductive resistance of the pipe material (Figure 8).

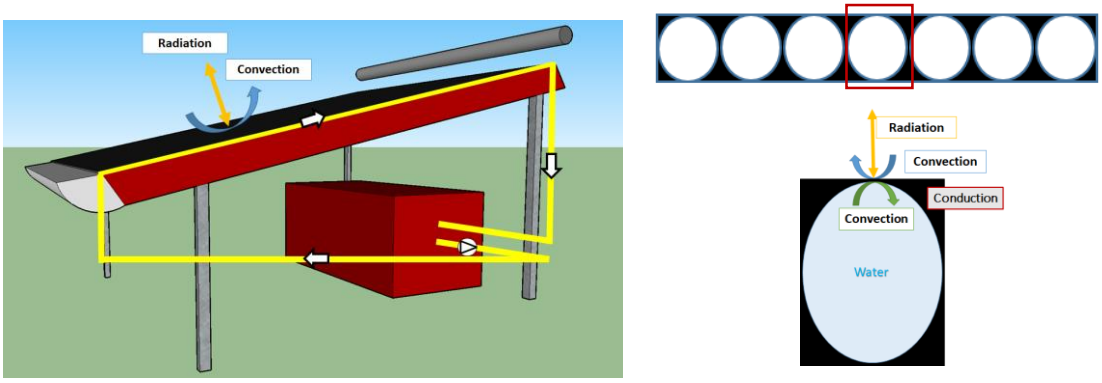

Figure 8. Heat transfer in operating mode 1 and cross-section of collector pipe

Theoretically, cooling based on water flowing down the collector surface (downflow, mode 2) would have greater cooling power than mode 1. In the former the water transfers heat directly to the cold source, eluding the adverse effect on heat transfer of internal convective and conductive thermal resistance. Furthermore, the direct contact between water and air in downflow mode gives rise to evaporative cooling (Figure 9), which favours heat dissipation.

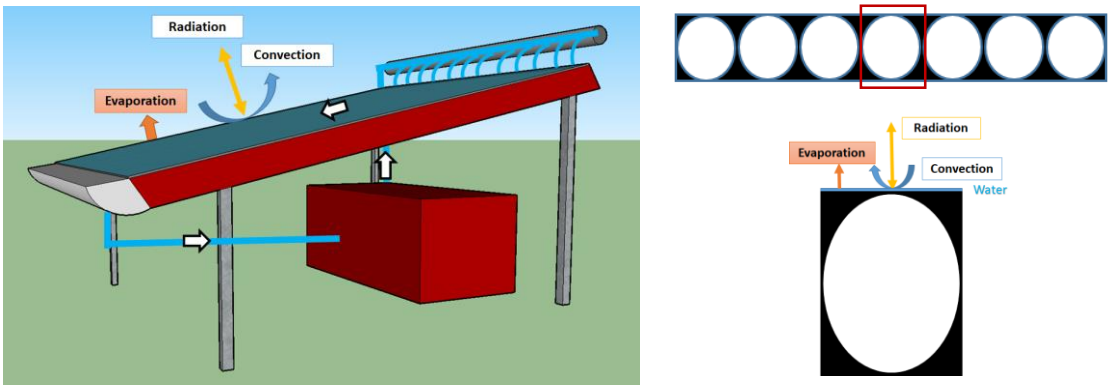

Figure 9. Heat transfer in operating mode 2 and cross-section of collector pipe

Consequently, the aim of the experimental trials conducted on the aforementioned system was to assess and compare the nocturnal cooling power of the two operating modes. Whereas operating mode 1 has been assessed and contrasted by earlier authors, operating mode 2 has not been previously researched. Given the enhancement of cooling power relative to mode 1 expected of mode 2, the latter was assessed and contrasted experimentally to conventional or mode 1 operation.

[redacted]Theoretical fundamentals

The Duffie and Beckman formula for calculating water temperature in a solar collector served as a basis for the radiation systems built [50]. In the operating mode 1 (in-pipe) energy balance for

the radiation panel, the useful nocturnal cooling power referred to the panel's convection-, radiation- and conduction-induced thermal loss from the fluid to the outdoor environment (T_{eq}). The equivalent temperature (T_{eq}, see section 2) identified the cold source in the convective-radiant transfer.

The variation in water energy with the system operating in mode 1 was found with Equation 2:

$$-m_w \cdot Cp_w \cdot \frac{dT_w}{dt} = Q_u \quad \text{(Eq.2)}$$

where m_w is the flow rate of the water circulating inside the pipes, Cp_w its specific heat, T_w water temperature and Q_u the useful nocturnal cooling energy in connection with panel convection-, radiation- and conduction-driven thermal loss. Useful energy was defined as in Equation 3:

$$Q_u = \frac{T_w - T_{eq}}{R_{conv\_i} + R_{cond} + R_{conv\_rad\_ext}} \quad \text{(Eq.3)}$$

where T_w is water temperature, T_{eq} the equivalent heat transfer temperature, R_{conv_i} the convective resistance to water circulation inside the pipes, R_{cond} the conductive resistance given the heat transfer generated across the polypropylene material and $R_{conv\_rad\_ext}$ outer convective-radiant resistance associated with convective and radiant heat loss to the outdoor environment (air, surrounds and sky).

As commented above, the equivalent heat transfer temperature (T_{eq}) is the minimum temperature that the water would reach under certain climatic conditions [46]. It was defined as in Equation 4:

$$T_{eq} = \frac{h_a \cdot T_a + h_{r\_surroundings} \cdot T_{surroundings} + h_{r\_sky} \cdot T_{sky}}{h_a + h_{r\_surroundings} + h_{r\_sky}} \quad \text{(Eq.4)}$$

where h_a is the outdoor convective heat transfer coefficient, T_a the outdoor air temperature, $h_{r\_surrounds}$ the radiant heat transfer coefficient characterising the radiant heat exchange between the panel surface and the surrounds, $T_{surrounds}$ the temperature in the surrounds, h_{r_sky} the radiant heat transfer coefficient characterising the radiant heat exchange between the panel surface and the sky and T_{sky} the sky temperature.

In the operating mode 2 (water flowing down the collector surface, downflow) energy balance for the radiation panel, the variation in the water energy depended on the panel's convection and radiation thermal loss from the fluid to the outdoor environment (Q_u). In addition, the direct water - air contact in that mode would give rise to evaporative cooling ($Q_{evaporative}$), favouring heat dissipation.

The variation in the water energy when the system was operating in mode 2 was found with Equation 5:

$$-m_w \cdot Cp_w \cdot \frac{dT_w}{dt} = Q_u + Q_{evaporative} \quad \text{(Eq.5)}$$

where m_w is the flow rate of the water flowing down the collector surface, Cp_w the specific heat of the water, T_w the water temperature, Q_u the useful nocturnal cooling attributable to convection and radiation thermal loss in the panel and $Q_{evaporative}$ the cooling energy attributable to evaporative cooling.

Useful nocturnal cooling energy attributable to panel convection and radiation thermal loss was found with Equation 6:

$$Q_u = \frac{T_w - T_{eq}}{R_{conv\_rad\_ext}} \quad \text{(Eq.6)}$$

where T_w is water temperature, T_{eq} equivalent heat transfer temperature and $R_{conv\_rad\_ext}$ outdoor convective-radiant resistance associated with convective and radiant heat loss to the outdoor environment (air, surrounds, sky).

Water evaporation-driven cooling consists in the diffusion of a given component, water vapour, in a stationary medium, air. The cooling energy attributable to evaporation was found with Equation 7 [51]:

$$Q_{evaporative} = \frac{K_m}{R} \cdot h_{fg} \cdot \left(\frac{P_{vs}(T_w)}{T_w} - RH \cdot \frac{P_{vs}(T_a)}{T_a}\right) \quad \text{(Eq.7)}$$

where K_m is the mass transfer coefficient, R the universal gas constant, h_{fg} the evaporation heat assessed at the temperature of the interface water, RH the relative humidity of the air and P_{vs} saturation pressure at the downflow water (T_w) and air (Ta) temperatures.

Mass transfer coefficient K_m was found relative to the outdoor convective heat transfer coefficient with Equation 8, applying the Chilton-Colburn analogy valid for flat panels and Pr, Sc>0.5 [52]:

$$K_m = \frac{\left(\frac{Sc}{Pr}\right)^{1/3}}{\rho \cdot Cp} \cdot ha \quad \text{(Eq.8)}$$

where K_m is the mass transfer coefficient, Sc the Schmidt number, Pr the Prandtl number, ρ and Cp air density and specific heat and h_a the outdoor convective heat transfer coefficient.

Thermal assessment variables in the experimental system

The monitoring scheme described in section 2 logged the tank water temperature (T_w), the collector thermal equivalent temperature (T_{eq}) and the outdoor weather conditions at 1 min intervals 24/7. The energy performance of the experimental system under both operating modes was assessed at 45 min intervals, based on the assumption that three-quarters of an hour would suffice for the tank water temperature to vary by 0.5 °C.

The values for the following variables were obtained for each 45 min interval:

$$Dissipated\ energy\ \ (Ed)[Wh] = \frac{\rho \cdot V \cdot Cp \cdot (T_w(t-1) - T_w(t))}{3600} \quad \text{(Eq.9)}$$

$$Transmission\ losses\ (Pt)[Wh] = UA \cdot (\overline{T_w} - \overline{T_a}) \cdot \Delta t \quad \text{(Eq.10)}$$

$$Mean\ collector\ dissipation\ power\ (Pd)\left[\frac{W}{m2}\right] = \frac{Ed - Pt}{\Delta t \cdot At} \quad \text{(Eq.11)}$$

where:

- Ed: energy dissipated in the system, found by measuring the tank water temperatures as described in section 2
- V: cumulative volume (200 L)
- ρ, Cp: water density and specific heat
- $Tw(t)$: tank water temperature at time *t*
- Pt: transmission loss in the tank due to the temperature difference between the water and the outdoor environment
- Δt: time increment, here the 45 min (0.75 h) intervals at which the system was thermally assessed
- UA [W/K]: tank heat transfer coefficient, found experimentally (section 4)
- $\overline{T_w}$: mean tank water temperature over Δt
- $\overline{T_a}$: mean air temperature over Δt
- At: panel transfer area (m^2).

In addition, evaporation in the downflow mode (mode 2) was quantified as the end-of-night loss of water volume.

System energy performance was compared in the two operating modes in terms of the collector's mean dissipation power (*Pd*), a parameter widely used in radiant panel heat capture and dissipation studies. It was obtained experimentally in both operating modes for different values of $\Delta T = \overline{T_w} - \overline{T_{eq}}$. ($\overline{T_w}$: mean tank water temperature over Δt; $\overline{T_{eq}}$: mean equivalent heat transfer temperature over Δ).

As noted in subsection 3.2, the difference between the water and equivalent convective-radiant heat transfer temperatures (Equation 6) governs the variation in useful nocturnal cooling energy attributable to convection- and radiation-driven thermal loss. Similarly, the difference in saturation pressures at the downflowing water and air temperatures determines evaporation-induced dissipation power. Given that air temperature was factored into the equivalent heat transfer temperature (Equation 4) and convection and mass transfer were inter-related further to Equation 8, the mean collector dissipation power, *Pd* (W/m2) (a parameter widely used in radiant heat panel capture and dissipation studies), was chosen as the variable to compare the system in the two operating modes for different setpoint values: $\Delta T = \overline{T_w} - \overline{T_{eq}}$, where $\overline{T_w}$ is the mean tank temperature over Δt and $\overline{T_{eq}}$ the mean equivalent heat transfer temperature over Δt.

4 Tests and results

The aim of the experimental trials conducted on the system described above was to assess and compare nocturnal cooling power in the radiation panel's two operating modes (Figure 1): operating mode 1, with water circulating inside the pipes and mode 2 in which it flowed down the collector surface (downflow). The experimental trials conducted and the respective findings are discussed in the following sub-sections.

[redacted] General

The tests run can be classified in terms of the secondary aim pursued:

- Test 0: characterisation of tank thermal losses (UA)
- Test 1: assessment of the mean nocturnal dissipation power in operating mode 1 for different tank set point temperatures
- Test 2: assessment of the mean nocturnal dissipation power in operating mode 2 for different tank setpoint temperatures.

All the tests were monitored using Labview software, which established system operating times and modes (in-pipe or downflow) for each test.

[redacted] Tests

4.2.1 Test 0: characterisation of tank thermal losses (UA)

This test was conducted to characterise the tank energy loss factor by quantifying the energy transferred from the storage tank to the environment during a given period of time. In this test, the water circulating in the pipes was heated from 11:00 to 19:00 with the system operating as a solar collector. When the water ceased to circulate after 19:00 the sole energy exchange possible was between the water and the outdoor environment across the storage tank walls (Figure 10). According to the manufacturer's specifications [53], the rate established for operation in this mode was 260 L/h.

Collection operating mode (11:00 to 19:00)	Dissipation operating mode (19:00 to 08:00)
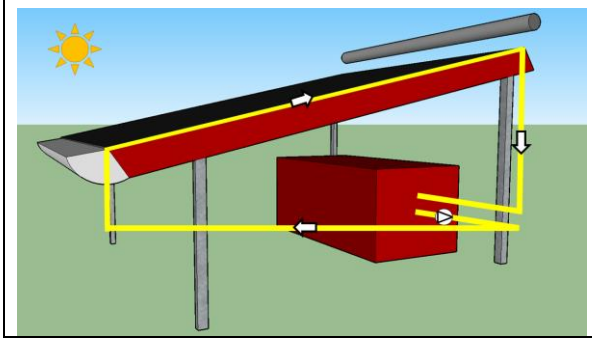	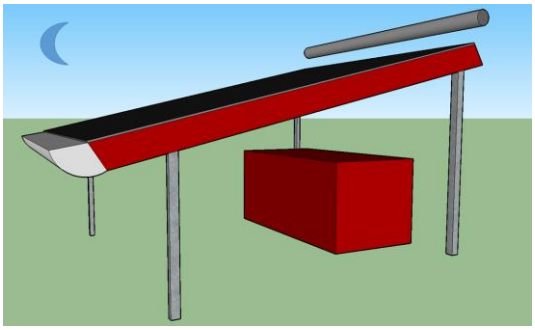

Figure 10. Test 0: characterisation of tank thermal losses (UA)

4.2.2 Test 1: assessment of the mean nocturnal dissipation power in operating mode 1 for different tank set point temperatures

Given the tank thermal loss factor (UA) for the water circulating inside the pipes at night, test 1 was conducted to assess the mean collector dissipation power, *Pd* (W/m2). That entailed defining a setpoint value as the ideal temperature of the water in the tank at cooling start-up (00:00). Daytime mode operation began at 14:00. From 14:00 to 14:30 pm the water circulation pump will be forced on. After 14:30, the mean tank temperature was automatically checked every 30 min and after the setpoint temperature was reached or exceeded the pump was switched off (Figure 11, left). At 00:00 the pump was turned back on, driving water continuously inside the pipes until 08:00 (Figure 11, right). As in test 0, the flow rate for collection and dissipation mode in test 1 was set at 260 L/h.

Collection mode (from 14:00 until setpoint T was reached)	Dissipation mode (00:00 to 08:00)
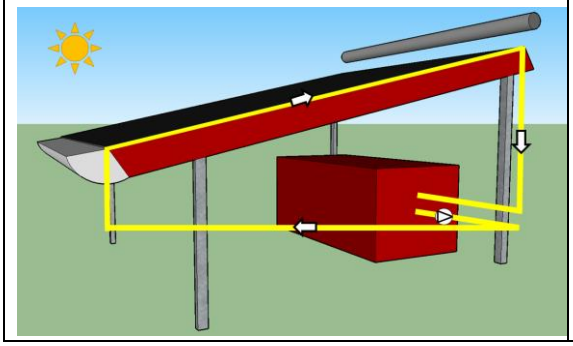	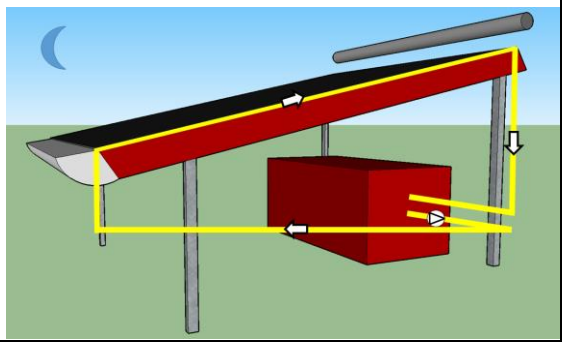

Figure 11. Type 1 test: assessing mean nocturnal dissipation power in operating mode 1

4.2.3 Test 2: assessment of the mean nocturnal dissipation power in operating mode 2 for different tank set point temperatures

Test 2 was conducted to assess the mean collector dissipation power, *Pd* (W/m2) for the water flowing over the collector (downflow), likewise on the grounds of the tank thermal loss factor (UA). As in test 1, that entailed defining a setpoint temperature and starting system daytime mode operation at 14:00. Here also, the pump was switched on between 14:00 and 14:30, after which the monitoring system checked the mean tank temperature every 30 min (Figure 12, left). Once the mean tank temperature was equal to or greater than the setpoint temperature, the pump was turned off and switched back on at 00:00, driving the water continuously down the collector surface until 08:00 (Figure 12, right). The flow required in the case of test 2 in dissipation mode has been calculated by obtaining the speed necessary to form a continuous downflow through the formulation of Bird [53]. The value obtained is 1440 L / h in dissipation mode. In the same way, an experimental flow evaluation test was performed to ensure that the reference flows of tests 1 and 2 are flows that make the system work optimally (that is, present the maximum possible dissipation power in similar climatic conditions) so that the comparison between the two (test 1 and 2) is carried out correctly ".

Collection mode (from 14:00 until set point T was reached)	Dissipation mode (00:00 to 08:00)
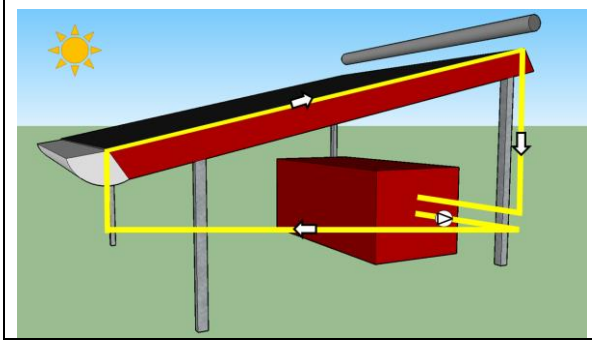	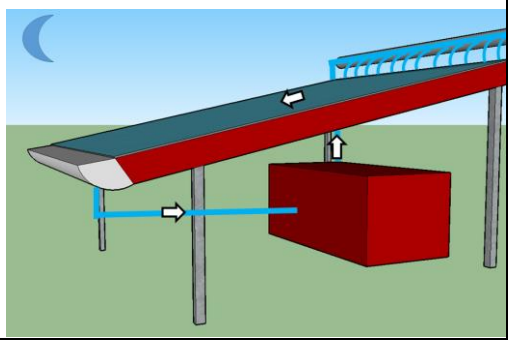

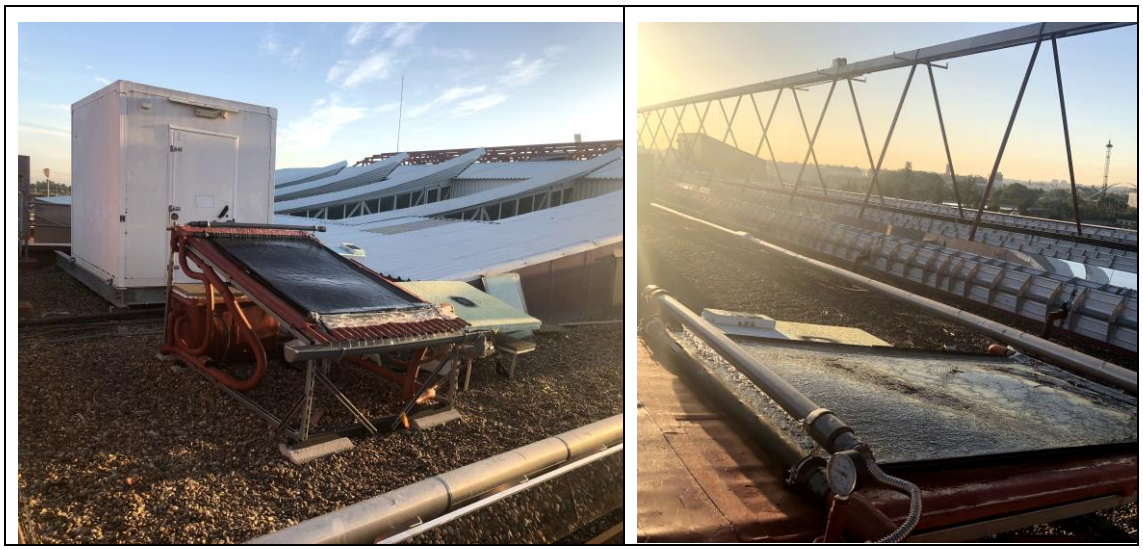

Figure 12. Type 2 test: assessing mean nocturnal dissipation power in operating mode 2

[redacted]Test programme

The tests described in sub-section 4.2 were conducted in Seville over 8 weeks in August and September 2019 (Table 1). Monitoring system preparation and testing, including thermocouple calibration and installation, data gathering system programming and Labview software operation verification, were conducted in July.

As Table 1 shows, test 0 was conducted during the first week to characterise and validate tank thermal losses. Once the UA was determined, tests 1 and 2 were undertaken with setpoint (cooling start-up) temperatures ranging from 26 °C to 32 °C to assess the nocturnal cooling power of the two modes of operation (in-pipe and downflow).

Table 1. Test programme (setpoint temperatures in °C)

Week 1	Day 1	Day 2	Day 3	Day 4	Day 5	Day 6	Day 7
	Test 0	Test 0	Test 0	Test 0	Test 0	Test 0	Test 0
Week 2	Day 1	Day 2	Day 3	Day 4	Day 5	Day 6	Day 7
	Test 2 (set point temperature 30)	Test 2 (set point temperature 26)	Test 2 (set point temperature 32)	Test 2 (set point temperature 28)	Test 1 (set point temperature 30)	Test 1 (set point temperature 30)	Test 1 (set point temperature 30)
Week 3	Day 1	Day 2	Day 3	Day 4	Day 5	Day 6	Day 7
	Test 2 (set point temperature 32)	Test 2 (set point temperature 28)	Test 2 (set point temperature 26)	Test 2 (set point temperature 32)	Test 1 (set point temperature 30)	Test 1 (set point temperature 30)	Test 1 (set point temperature 30)
Week 4	Day 1	Day 2	Day 3	Day 4	Day 5	Day 6	Day 7
	Test 2 (set point temperature 30)	Test 2 (set point temperature 26)	Test 2 (set point temperature 32)	Test 2 (set point temperature 28)	Test 1 (set point temperature 26)	Test 1 (set point temperature 26)	Test 1 (set point temperature 26)
Week 5	Day 1	Day 2	Day 3	Day 4	Day 5	Day 6	Day 7
	Test 2 (set point temperature 28)	Test 2 (set point temperature 30)	Test 2 (set point temperature 26)	Test 2 (set point temperature 32)	Test 1 (set point temperature 28)	Test 1 (set point temperature 28)	Test 1 (set point temperature 28)
Week 6	Day 1	Day 2	Day 3	Day 4	Day 5	Day 6	Day 7
	Test 2 (set point temperature 28)	Test 2 (set point temperature 30)	Test 2 (set point temperature 26)	Test 2 (set point temperature 32)	Test 1 (set point temperature 32)	Test 1 (set point temperature 32)	Test 1 (set point temperature 32)
Week 7	Day 1	Day 2	Day 3	Day 4	Day 5	Day 6	Day 7
	Test 2 (set point temperature 32)	Test 2 (set point temperature 28)	Test 2 (set point temperature 26)	Test 2 (set point temperature 32)	Test 1 (set point temperature 30)	Test 1 (set point temperature 30)	Test 1 (set point temperature 30)
Week 8	Day 1	Day 2	Day 3	Day 4	Day 5	Day 6	Day 7

	Test 2 (set point temperature 28)	Test 2 (set point temperature 32)	Test 2 (set point temperature 30)	Test 2 (set point temperature 26)	Test 1 (set point temperature 26)	Test 1 (set point temperature 26)	Test 1 (set point temperature 26)

ResultThe results of the experimental study are presented below. For this, a representative sample of days has been selected in order to show the main results in detail and the conclusions obtained from the complete experimental study.

4.3.1 Test 0

As noted, this test was conducted to characterise the tank energy loss factor by quantifying the energy transferred from the storage tank to the environment during a given period of time (UA).

The water was heated by circulating it inside the collector pipes from 11:00 to 19:00. As the water ceased to circulate after 19:00, the sole energy exchange possible was between the water and the outdoor environment across the storage tank walls. The graph in Figure 13 shows the variation in the water, air and equivalent temperatures during test 0 over several consecutive days. After the system had operated in collector mode from 11:00 to 19:00, the tank water temperature rose by approximately 15 °C, with heat subsequently dissipating to the outdoor environment across the tank walls.

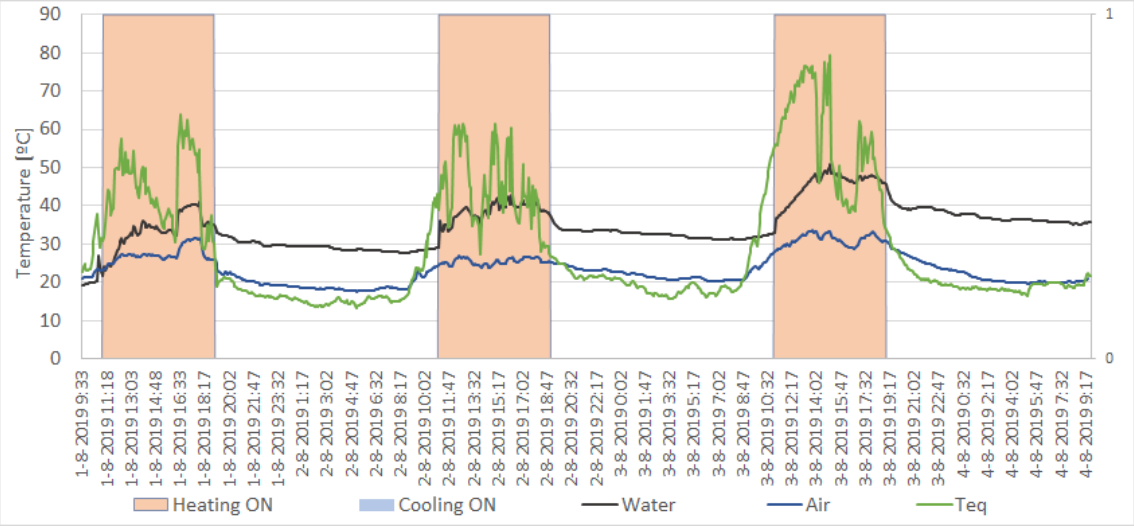

Figure 13. Variation in temperature over 4 days in August 2019, test 0

The mean tank water temperature, mean air temperature and energy dissipated to the air were obtained over 45 min intervals to characterise tank thermal loss. Since the sole energy exchange possible was between the water and the outdoor environment across the tank walls, the thermal loss factor for each 45 min interval was found with Equation 12:

$$Dissipated\ energy\ (Ed)[Wh] = Transmission\ loss\ [Wh]$$

$$\frac{\rho \cdot V \cdot Cp \cdot (T_w(t-1) - T_w(t))}{3600} = UA \cdot (\overline{T_w} - \overline{T_a}) \cdot \Delta t \qquad \text{(Eq.12)}$$

The mean 7 day UA found, characterised and validated (Table 1) came to 4.5 W/K, with an 85th percentile value of 5.3 W/K and a 15th percentile value of 3.9 W/K.

4.3.2 Test 1

Figure 14 below graphs the variation in temperature across 3 consecutive test 1 days for a setpoint water temperature of 30 °C.

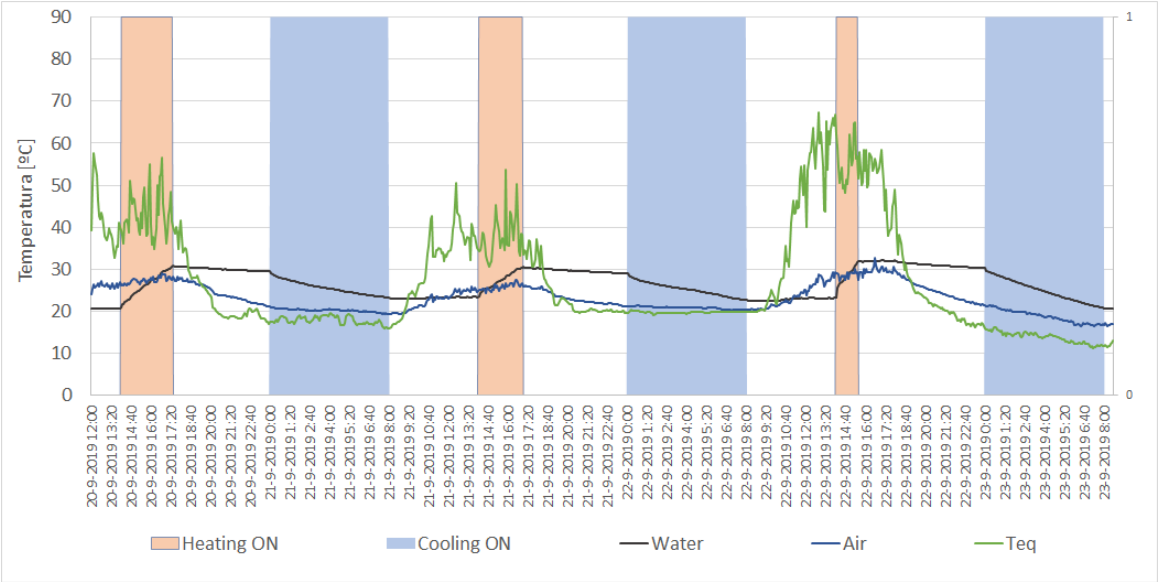

Figure 14. Variation in temperature over 3 days in September 2019, test 1

One-half hour after system start-up time, i.e., at 14:30, the monitoring system checked the mean temperature of the tank water every 30 min. As the system shut down after the mean T was equal to or greater than the setpoint, collection mode duration differed on the 3 test days. As Figure 14 shows, overnight, with the water circulating continuously inside the pipes from 00:00 to 08:00, water temperature declined by approximately 7 °C on the first 2 days, but by around 10 °C on the third. That difference can be explained by the lower equivalent heat transfer temperature on the third night.

The energy dissipation and mean nocturnal dissipation power values during system operation on the three nights graphed in Figure 14 are listed in Tables 2, 3 and 4. Further to the data in Table 2 for the night of 21 September, the mean initial water temperature at dissipation start-up of 29.5 °C declined to 23.5 °C, with a total energy dissipation of 1.3 kWh at the equivalent temperature and relative humidity given in the table. The 17.9 °C equivalent temperature at the outset dipped during the night to 17.3 °C, while relative humidity rose from 82 to 84%.

Table 2. Test 1 data for 21 September

	TEST 1-21 September (Set point temperature 30 °C)						
	Water temperature (Tw) [°C]	Equivalent temperature (Teq) [°C]	Air temperature (Ta) [°C]	Relative humidity (HR)	Energy dissipated [Wh]	Heat transfer loss in tank [Wh]	Dissipation power (Pd) [W/m2]
00:00:00	29.5						
00:45:00	27.9	17.9	20.9	0.82	353.0	30.3	204.8
01:35:00	27.2	17.9	20.6	0.82	159.4	27.7	83.6
02:25:00	26.4	18.4	20.5	0.83	152.9	25.1	81.1
03:15:00	25.8	18.1	20.2	0.85	121.7	23.3	62.5
04:05:00	25.4	19.0	20.4	0.83	96.6	20.7	48.2
04:55:00	24.8	18.1	20.3	0.82	126.0	18.9	68.0
05:45:00	24.4	18.4	20.2	0.82	84.6	17.2	42.8
06:35:00	23.9	17.1	20.0	0.84	103.1	16.2	55.2
07:25:00	23.5	17.3	19.7	0.84	71.7	15.6	35.6

Tables 3 and 4 give analogous findings for the nights of 22 and 23 September. The energy dissipated during the former was 1.3 kWh and 1.9 kWh in the latter. The value for 23 September was greater than for the other two nights because the minimum equivalent convective-radiant

transfer temperature (T_{eq}) of 11.8 °C was much lower than the 17.3 °C and 19.9 °C recorded on 21 and 22 September, respectively.

Table 3. Test 1 data for 22 September

	TEST 1-22 September (Set point temperature 30 °C)						
	Water temperature (Tw) [°C]	Equivalent temperature (Teq) [°C]	Air temperature (Ta) [°C]	Relative humidity (HR)	Energy dissipated [Wh]	Heat transfer loss in tank [Wh]	Dissipation power (Pd) [W/m2]
00:00:00	29.0						
00:45:00	27.5	20.1	21.3	0.90	359.2	26.8	211.1
01:35:00	26.7	19.8	21.2	0.90	148.7	23.0	79.8
02:25:00	26.1	19.6	21.0	0.90	123.4	21.3	64.9
03:15:00	25.6	19.7	21.0	0.90	106.7	19.1	55.6
04:05:00	25.2	19.6	21.1	0.89	85.6	17.3	43.4
04:55:00	24.7	19.8	20.9	0.90	101.8	15.9	54.5
05:45:00	24.2	19.7	21.0	0.91	102.0	14.0	55.8
06:35:00	23.5	19.9	20.4	0.93	98.2	12.8	54.2
07:25:00	22.9	19.9	20.4	0.96	91.8	11.4	50.5

As the night of 22 September (Table 3) was partially cloudy according to the sky meter data, the equilibrium temperature was similar to the outdoor air temperature and the relative humidity values recorded were high. Those conditions generated mean dissipation power values just over half (60 %) of those observed on 23 September (Table 4). As Table 4 shows, on a night with fairly clear skies, the mean power value was on the order of 100 W/m^2, a figure given in the literature reviewed as a means to be expected under ideal climate conditions.

Table 4. Test 1 data for 23 September

	TEST 1-23 September (Set point temperature 30 °C)						
	Water temperature (Tw) [°C]	Equivalent temperature (Teq) [°C]	Air temperature (Ta) [°C]	Relative humidity (HR)	Energy dissipated [Wh]	Heat transfer loss in tank [Wh]	Dissipation power (Pd) [W/m2]
00:00:00	30.3						
00:45:00	28.7	15.8	21.2	0.64	427.3	31.8	248.3
01:35:00	27.7	14.9	20.2	0.68	218.9	30.4	119.7
02:25:00	26.6	14.4	19.9	0.70	218.4	28.1	120.8
03:15:00	25.6	14.7	19.4	0.68	211.4	25.5	118.0
04:05:00	24.7	14.1	18.7	0.69	199.1	24.1	111.1
04:55:00	23.7	14.2	18.3	0.69	194.9	22.0	109.7
05:45:00	22.8	13.1	17.7	0.71	187.3	21.6	105.2
06:35:00	22.0	12.5	17.1	0.74	179.8	21.4	100.6
07:25:00	21.2	11.8	16.8	0.75	153.8	18.4	85.9

4.3.3 Test 2

The variation in temperature across 4 consecutive test 2 days with water setpoint temperatures of 32 °C, 28 °C, 26 °C and 32 °C is graphed in Figure 15.

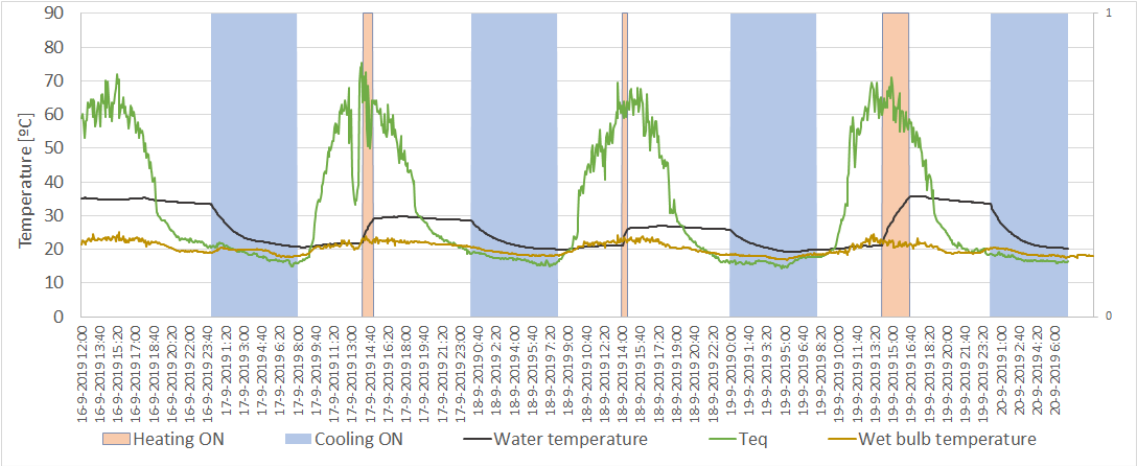

Figure 15. Variation in temperature over 4 days in September 2019, test 2

As in test 1, after start-up at 14:00 water was pumped through the pipes in collection mode for as long as necessary to reach the set point at temperature established. At 00:00 downflow mode was activated, with the water flowing continuously down the collector surface until 08:00.

On the first day shown in the figure, the temperature dropped during downflow mode operation by 13 °C from the setpoint 32 °C and on the subsequent days by 8.6 °C (from 28 °C), 5.92 °C (from 26 °C) and 13.2 °C (from 32 °C). As expected, the decline in water temperature during operation in dissipation mode depended on the setpoint and cold source temperatures (convective-radiant in test 1 and convective-radiant-evaporative in test 2).

The energy dissipation and mean nocturnal dissipation power values during system operation on the four nights graphed in Figure 15 are given below. Further to the data in Table 5 for the night of 17 September, the mean initial water temperature at dissipation start-up of 33.4 °C declined to 20.9 °C, with a total energy dissipation of 2.6 kWh at the equivalent temperature and relative humidity given in the table. The 21.1 °C equivalent temperature at the outset dipped overnight to 16.2 °C, whilst relative humidity rose from 63 to 84%. The steeper drop in temperature soon after dissipation mode operation began was due to the loss, later in the night, of evaporative cooling power as the difference between the water and the air declined and relative humidity rose. On 17 September, 2.5 % of the tank water evaporated between 00:00 and 08:00 (based on the overnight volume loss, sub-section 4.2).

Table 5. Test 2 data for 17 September

	TEST 2-17 September (Set point temperature 32 °C)						
	Water temperature (Tw) [°C]	Equivalent temperature (Teq) [°C]	Air temperature (Ta) [°C]	Relative humidity (HR)	Energy dissipated [Wh]	Heat transfer loss in tank [Wh]	Dissipation power (Pd) [W/m2]
00:00:00	33.4						
00:45:00	29.7	21.1	24.5	0.63	839.6	27.3	515.7
01:35:00	26.7	21.2	24.0	0.66	620.8	16.2	383.9
02:25:00	24.5	19.9	22.5	0.72	452.2	11.8	279.7
03:15:00	23.2	19.2	21.8	0.75	270.0	7.7	166.5
04:05:00	22.5	18.5	21.5	0.76	149.0	5.2	91.3
04:55:00	22.2	17.8	21.4	0.77	64.4	3.7	38.6
05:45:00	21.7	16.8	21.1	0.79	112.4	3.3	69.3
06:35:00	21.2	16.6	20.5	0.81	97.7	3.7	59.7
07:25:00	20.9	16.2	20.1	0.84	67.6	3.7	40.6

During the night of 18 September (Table 6) the mean initial water temperature at dissipation start-up of 33.4 °C declined to 20.9 °C, with a total energy dissipation of 2.6 kWh at the equivalent temperature and relative humidity given in the table. A total of 2.2 % of the water in the tank evaporated on that date.

Table 6. Test 2 data for 18 September

	TEST 2-18 September (Set point temperature 28 °C)						
	Water temperature (Tw) [°C]	Equivalent temperature (Teq) [°C]	Air temperature (Ta) [°C]	Relative humidity (HR)	Energy dissipated [Wh]	Heat transfer loss in tank [Wh]	Dissipation power (Pd) [W/m2]
00:00:00	28.6						
00:45:00	26.1	19.0	23.0	0.70	576.9	16.6	355.8
01:35:00	24.3	18.5	21.9	0.72	379.4	12.2	233.1
02:25:00	22.9	17.5	21.4	0.76	278.0	8.5	171.1
03:15:00	22.0	17.3	20.7	0.79	195.2	6.5	119.8
04:05:00	21.3	17.1	20.1	0.82	143.8	5.6	87.7
04:55:00	20.7	17.0	19.7	0.84	121.3	4.9	73.9
05:45:00	20.3	16.4	19.4	0.85	63.7	4.2	37.8
06:35:00	20.2	15.6	19.4	0.85	25.8	3.6	14.1
07:25:00	20.1	15.6	19.2	0.86	26.3	3.7	14.4

The findings for the night of 19 September (Table 7) showed that the mean temperature at cooling start-up, 28.6 °C, declined to 19.2 °C, whilst 1.4 kWh of energy was dissipated and 2.3 % of the water in the tank evaporated.

Table 7. Test 2 data for 19 September

	TEST 2-19 September (Set point temperature 26 °C)						
	Water temperature (Tw) [°C]	Equivalent temperature (Teq) [°C]	Air temperature (Ta) [°C]	Relative humidity (HR)	Energy dissipated [Wh]	Heat transfer loss in tank [Wh]	Dissipation power (Pd) [W/m2]
00:00:00	25.8						
00:45:00	23.7	16.2	20.5	0.75	501.8	16.1	308.4
01:35:00	22.2	15.9	19.7	0.77	304.8	12.3	185.7
02:25:00	21.2	15.9	19.3	0.82	198.6	9.3	120.2
03:15:00	20.5	16.5	19.3	0.85	143.4	6.2	87.1
04:05:00	19.8	15.8	18.8	0.86	140.7	5.2	86.0
04:55:00	19.4	15.0	18.4	0.85	92.1	4.6	55.6
05:45:00	19.2	15.4	18.4	0.86	29.3	3.6	16.3
06:35:00	19.5	17.0	18.8	0.86	0.0	2.1	0.0
07:25:00	19.8	17.6	19.1	0.85	0.0	2.1	0.0

As the data in Table 8 for the night of 20 September show, the mean initial dissipation start-up temperature, 33.5 °C, declined to 20.2 °C, with a total energy dissipation of 2.8 kWh at the equivalent temperature and relative humidity given in the table, whilst evaporation accounted for 2.6 % of the total tank volume.

Table 8. Test 2 data for 20 September

	TEST 2-20 September (Set point temperature 32 °C)						
	Water temperature (Tw) [°C]	Equivalent temperature (Teq) [°C]	Air temperature (Ta) [°C]	Relative humidity (HR)	Energy dissipated [Wh]	Heat transfer losses in the tank [Wh]	Dissipation power (Pd) [W/m2]
00:00:00	33.5						
00:45:00	29.0	18.4	22.4	0.67	1059.4	34.4	650.8
01:35:00	25.8	18.2	21.8	0.70	635.4	21.1	390.1
02:25:00	23.7	17.8	21.2	0.74	428.9	13.5	263.8

03:15:00	22.1	17.0	20.2	0.80	316.1	10.1	194.3
04:05:00	21.3	16.7	19.8	0.84	174.9	7.2	106.5
04:55:00	20.8	16.6	19.8	0.85	100.1	4.8	60.5
05:45:00	20.5	16.5	19.7	0.86	65.9	3.6	39.5
06:35:00	20.3	16.1	19.5	0.87	22.2	3.4	11.9
07:25:00	20.2	16.4	19.2	0.87	38.8	4.1	22.0

In addition to the specific findings, a review of Tables 5, 6, 7 and 8 revealed an overall pattern. Night-time operation exhibited two periods: the first when dissipation rates were higher, for both convection-radiation and evaporation were effective and a second when evaporative power began to wane, while the radiant effect was only observed as the proximity between the water and outdoor air temperatures. Those observations are suggestive of the possibility of hybridising modes 2 and 1: mode 2, downflow, during the early hours followed by mode 1 toward the end of the night in the absence of evaporation, drawing from convective-radiant mechanisms only.

5 Comparison of operating modes during dissipation

As noted in subsection 3.2, the variation in useful nocturnal cooling energy attributable to convection- and radiation-driven thermal loss would depend primarily on the difference between the water and equivalent convective-radiant heat transfer temperatures (Equation 6). Similarly, evaporation-induced dissipation power would depend on the difference in saturation pressures at the downflowing water and air temperatures. Given that air temperature was factored into the equivalent heat transfer temperature (Equation 4) and convection and mass transfer were inter-related further to Equation 8, the mean collector dissipation power, *Pd* (W/m2) was chosen as the variable to compare the system in the two operating modes for different values of

$\Delta T = \overline{T_w} - \overline{T_{eq}}$. ($\overline{T_w}$:

mean tank water temperature over

Δt, $\overline{T_{eq}}$:

mean equivalent heat transfer temperature over Δt=45 min. The graph in Figure 16 compares operating modes 1 and 2 during dissipation in terms of the mean nocturnal dissipation power found for different ΔT values in tests 1 and 2.

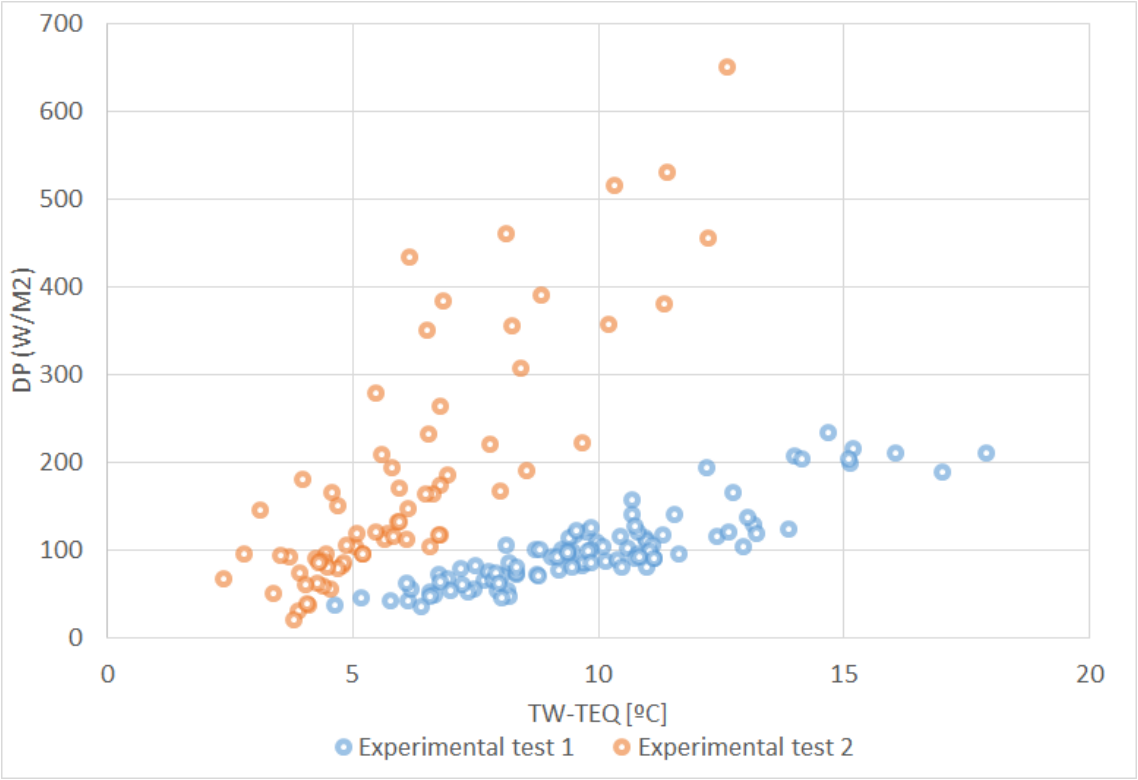

Figure 16. Dissipation power (DP) vs T_w-T_{eq} (°C)

As the figure shows, downflow cooling (test 2) exhibited greater cooling power than in-pipe cooling (test 1). As anticipated in sub-section 3.1, in the former the water transferred heat directly to the cold sources, eluding the adverse effect on heat transfer of internal convective and conductive (across the solid) thermal resistance. Furthermore, downflow along the surface of the collector enhanced convective cooling and the direct contact between water and air in that operating mode gave rise to evaporative cooling (Figure 9), which favoured heat dissipation.

Evaporative cooling was more effective, however, in the early hours of operation when the difference in temperature between water and air was wider and relative humidity lower. Consequently, a wide water temperature - equivalent heat transfer temperature differences, downflow was much more effective than in-pipe operation, with dissipation power values up to five-fold higher in test 2 than in test 1 (Figure 16). Likewise, as noted above, the pattern observed in the two-point clouds in the figure suggests that at narrow temperature differences (under 2.5 °C) operating mode 1 (in-pipe) exhibited higher performance.

The mean energy dissipated daily throughout the in-pipe test programme described in Table 1 (test 1) was 1.3 kWh, with an 85th percentile value of 1.6 kWh and a 15th percentile value of 1.1 kWh. Those means were substantially lower than the 2.3 kWh with an 85th percentile of 2.7 kWh and a 15th percentile of 1.8 kWh for the downflow mode (Figure 17). The mass of water evaporating in operating mode 2 came to a mean 2.5 % (2.4 L/m^2) across the entire suite of trials. Pearlmutter et al. [54], experimenting with different rooftop pond setups, reported water consumption ranging from moderate (2 L/m^2) to high (5 L/m^2) and dissipation power values of around 50 W/m^2. The 2.4 L/m^2 loss observed here was consequently deemed sufficiently low relative to the increase in dissipation power delivered.

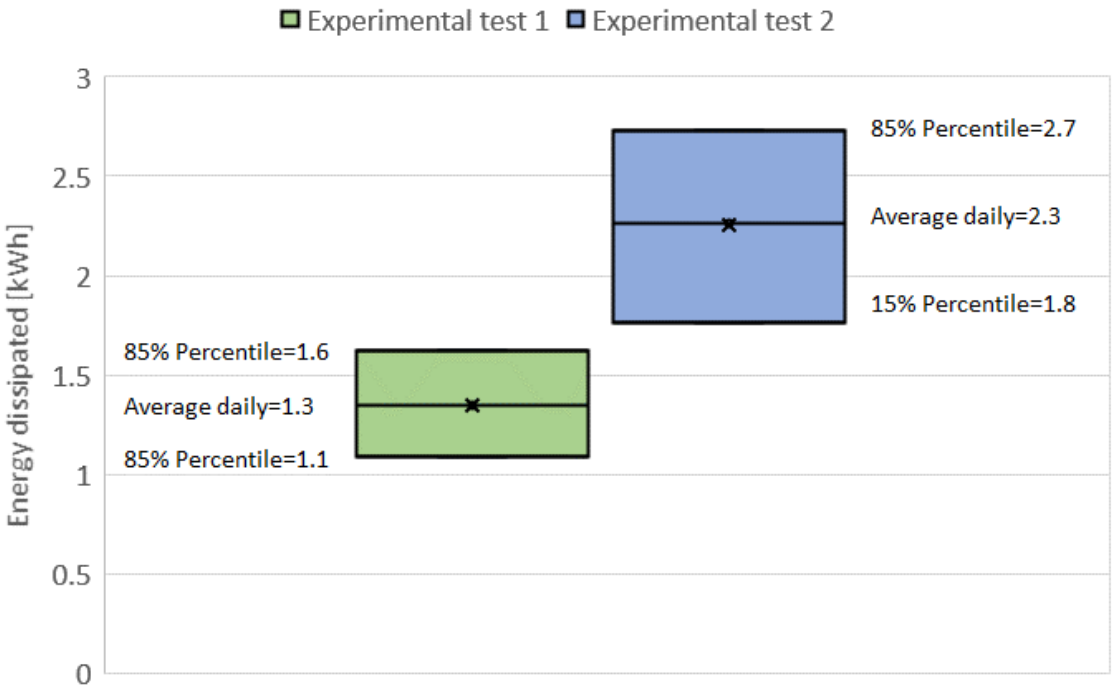

Figure 17. Energy dissipated in tests 1 and 2

At the end of the test programme set out in Table 1, an additional trial was conducted in which the collection and dissipation periods were of the same duration in both operating modes with a view to analysing system collection efficiency. The findings are shown in Figure 18.

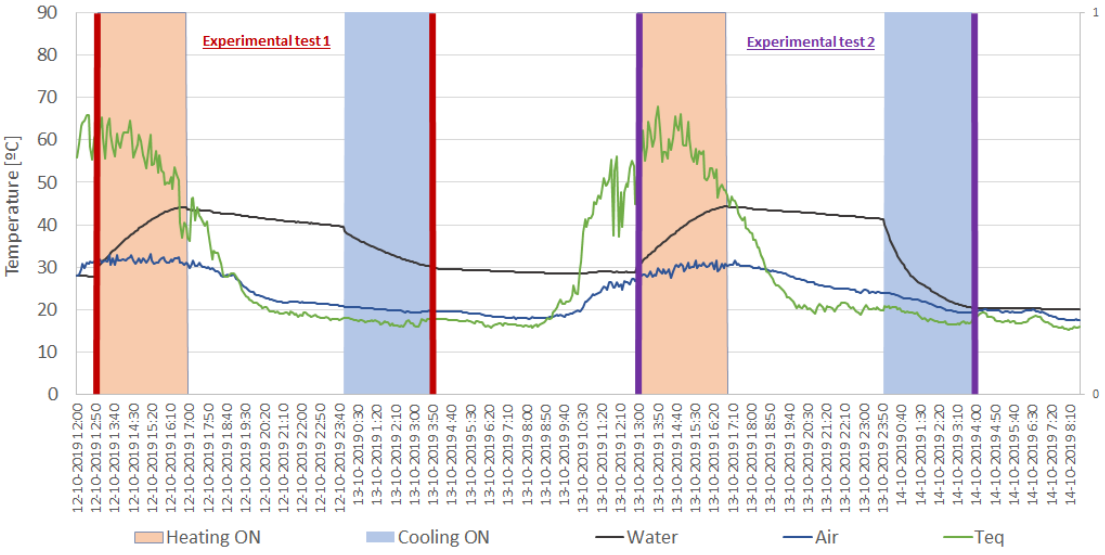

Figure 18. Collection and dissipation findings for tests 1 and 2

On the first day of that trial (Figure 18), the water circulated inside the pipes during collection and dissipation both. As the graph in the figure shows, under those conditions, the increase in water temperature during collection (approximately 13 °C) was greater than the decline during dissipation (around 10 °C). On the second day, with the water circulating inside the pipes during collection and flowing down the collector surface during dissipation, the increase in water temperature during collection (approximately 13 °C) was lesser than the decline during

dissipation (around 20 °C). Moreover, given a similar set point and climate conditions, the decline in temperature in test 2 (downflow) was two-fold greater than in test 1 (in-pipe).

6 Conclusions

The potential of the sky as a natural heat sink is limitless and on nights with fair weather, its temperature is lower than that of other environmental sinks (soil and air). The sky's promise as an environmental heat sink prompted this exploration of the potential of nocturnal radiation cooling. A review of the state of the art revealed that in all the radiative dissipators developed and tested to date the dissipation fluid (water) transferred heat indirectly to the heat sink (the sky) by circulating water inside solar collector pipes. The highest dissipation power values reported in the literature were on the order of 100 W/m^2.

Whilst in-pipe nocturnal dissipation has been analysed by earlier authors, downflow systems have not been researched. Given the foreseeable increase in cooling power in the latter operating mode, the aim sought in this study was to experimentally assess the nocturnal dissipation power of a downflow system and compare its cooling power to that of conventional in-pipe setups.

The foreseeable enhancement of cooling power in the downflow operating mode was compared experimentally to the conventional setup.

The most prominent conclusions drawn from the experimental findings are listed below.

- The rise in cooling power attributable to evaporative cooling was greater in the early hours of operation when the difference in temperature between water and air was wider and relative humidity lower. At wide differences between the water and equivalent heat transfer temperatures, dissipation power was observed to be up to five-fold higher in test 2 (downflow) than in test 1 (in-pipe).
- The mean energy dissipated daily in the in-pipe setup was 1.3 kWh, with an 85th percentile value of 1.6 kWh and a 15th percentile value of 1.1 kWh for the entire suite of tests conducted. Those means were substantially lower than the 2.3 kWh with an 85th percentile of 2.7 kWh and a 15th percentile of 1.8 kWh for the downflow mode.
- Possibility of hybridising modes: downflow during the first hours of the night followed by the conventional operating mode towards the end of the night given the evaporative power reduction.
- In downflow operating mode mean overnight (00:00 h to 08:0) water consumption was 2.4 L/m^2, a loss deemed to be satisfactory relative to the power gains delivered.

7 Acknowledgements

This study was funded by the Spanish Ministry of the Economy and Competitiveness under DACAR project 'Zero-Energy Balance Districts through Algorithms of Adaptive Comfort and Optimal Management of Energy Networks' (BIA2016-77431-C2-2-R); the ERDF under Urban Innovative Actions programme CartujaQanat project (UIA03-301) 'Recovering Street life in a Climate-Changing World'; and the University of Seville under Research Plan VI (VPPI-US).

8 References

[1] M. Santamouris, “Innovating to zero the building sector in Europe: Minimising the energy consumption, eradication of the energy poverty and mitigating the local climate change,” *Sol. Energy*, vol. 128, pp. 61–94, 2016.

[2] A. Mohajerani, J. Bakaric, and T. Jeffrey-Bailey, “The urban heat island effect, its causes, and mitigation, with reference to the thermal properties of asphalt concrete,” *J. Environ. Manage.*, vol. 197, pp. 522–538, 2017.

[3] M. Santamouris, “Cooling the buildings – past, present and future,” *Energy Build.*, vol. 128, pp. 617–638, 2016.

[4] D. K. Bhamare, M. K. Rathod, and J. Banerjee, “Passive cooling techniques for building and their applicability in different climatic zones—The state of art,” *Energy Build.*, vol. 198, pp. 467–490, 2019.

[5] F. Jomehzadeh *et al.*, “A review on windcatcher for passive cooling and natural ventilation in buildings, Part 1: Indoor air quality and thermal comfort assessment,” *Renew. Sustain. Energy Rev.*, vol. 70, no. November 2016, pp. 736–756, 2017.

[6] A. Aflaki, N. Mahyuddin, Z. Al-Cheikh Mahmoud, and M. R. Baharum, “A review on natural ventilation applications through building façade components and ventilation openings in tropical climates,” *Energy Build.*, vol. 101, pp. 153–162, 2015.

[7] N. Zhu, S. Li, P. Hu, F. Lei, and R. Deng, “Numerical investigations on performance of phase change material Trombe wall in building,” *Energy*, vol. 187, p. 116057, 2019.

[8] M. Rabani and M. Rabani, “Heating performance enhancement of a new design trombe wall using rectangular thermal fin arrays: An experimental approach,” *J. Energy Storage*, vol. 24, no. June, p. 100796, 2019.

[9] L. Shi, G. Zhang, W. Yang, D. Huang, X. Cheng, and S. Setunge, “Determining the influencing factors on the performance of solar chimney in buildings,” *Renew. Sustain. Energy Rev.*, vol. 88, no. September 2017, pp. 223–238, 2018.

[10] C. Jiménez-Xamán *et al.*, “Solar chimneys with a phase change material for buildings: An overview using CFD and global energy balance,” *Energy Build.*, vol. 186, pp. 384–404, 2019.

[11] J. Gao, A. Li, X. Xu, W. Gang, and T. Yan, “Ground heat exchangers: Applications, technology integration and potentials for zero energy buildings,” *Renew. Energy*, vol. 128, pp. 337–349, 2018.

[12] J. L. M. Simos Yannas, Evyatar Erell, *Roof Cooling Techniques*. 2006.

[13] J. Romaní, A. De Gracia, and L. F. Cabeza, “Simulation and control of thermally activated building systems (TABS),” *Energy Build.*, vol. 127, pp. 22–42, 2016.

[14] Y. Fang, J. Niu, and S. Deng, “An analytical technique for the optimal designs of tube-in-tank thermal energy storage systems using PCM,” *Int. J. Heat Mass Transf.*, vol. 128, pp. 849–859, 2019.

[15] L. Navarro, A. De Gracia, A. Castell, S. Álvarez, and L. F. Cabeza, “PCM incorporation in a concrete core slab as a thermal storage and supply system: Proof of concept,” *Energy Build.*, vol. 103, pp. 70–82, 2015.

[16] L. Navarro, A. De Gracia, A. Castell, S. Álvarez, and L. F. Cabeza, “Design of a prefabricated

concrete slab with PCM inside the hollows," *Energy Procedia*, vol. 57, pp. 2324–2332, 2014.

[17] S. Álvarez, L. F. Cabeza, A. Ruiz-Pardo, A. Castell, and J. A. Tenorio, "Building integration of PCM for natural cooling of buildings," *Appl. Energy*, vol. 109, pp. 514–522, 2013.

[18] J. Gao, A. Li, X. Xu, W. Gang, and T. Yan, "Ground heat exchangers: Applications, technology integration and potentials for zero energy buildings," *Renew. Energy*, vol. 128, pp. 337–349, 2018.

[19] P. Tewari, S. Mathur, and J. Mathur, "Thermal performance prediction of office buildings using direct evaporative cooling systems in the composite climate of India," *Build. Environ.*, vol. 157, no. April, pp. 64–78, 2019.

[20] G. Chiesa and M. Grosso, "Direct evaporative passive cooling of building. A comparison amid simplified simulation models based on experimental data," *Build. Environ.*, vol. 94, no. P1, pp. 263–272, 2015.

[21] M. S. Buker, B. Mempouo, and S. B. Riffat, "Experimental investigation of a building integrated photovoltaic/thermal roof collector combined with a liquid desiccant enhanced indirect evaporative cooling system," *Energy Convers. Manag.*, vol. 101, pp. 239–254, 2015.

[22] U. Berardi, P. La Roche, and J. M. Almodovar, "Water-to-air-heat exchanger and indirect evaporative cooling in buildings with green roofs," *Energy Build.*, vol. 151, pp. 406–417, 2017.

[23] M. Hanif, T. M. I. Mahlia, A. Zare, T. J. Saksahdan, and H. S. C. Metselaar, "Potential energy savings by radiative cooling system for a building in tropical climate," *Renew. Sustain. Energy Rev.*, vol. 32, pp. 642–650, 2014.

[24] J. Khedari, J. Waewsak, S. Thepa, and J. Hirunlabh, "Field investigation of night radiation cooling under tropical climate," *Renew. Energy*, vol. 20, no. 2, pp. 183–193, 2000.

[25] K. Panchabikesan, K. Vellaisamy, and V. Ramalingam, "Passive cooling potential in buildings under various climatic conditions in India," *Renew. Sustain. Energy Rev.*, vol. 78, no. March 2016, pp. 1236–1252, 2017.

[26] J. Hollick, "Nocturnal radiation cooling tests," *Energy Procedia*, vol. 30, no. 2011, pp. 930–936, 2012.

[27] M. G. Meir, J. B. Rekstad, and O. M. LØvvik, "A study of a polymer-based radiative cooling system," *Sol. Energy*, vol. 73, no. 6, pp. 403–417, 2002.

[28] H. S. Bagiorgas and G. Mihalakakou, "Experimental and theoretical investigation of a nocturnal radiator for space cooling," *Renew. Energy*, vol. 33, no. 6, pp. 1220–1227, 2008.

[29] M. Santamouris and D. Kolokotsa, "Passive cooling dissipation techniques for buildings and other structures: The state of the art," *Energy Build.*, vol. 57, pp. 74–94, 2013.

[30] M. Cucumo, S. Cucumo, L. Montoro, and A. Vulcano, "A one-dimensional transient analytical model for earth-to-air heat exchangers, taking into account condensation phenomena and thermal perturbation from the upper free surface as well as around the buried pipes," *Int. J. Heat Mass Transf.*, vol. 51, no. 3–4, pp. 506–516, 2008.

[31] "https://www.iea.org/weo/water/." .

[32] L. Evangelisti, C. Guattari, and F. Asdrubali, "On the sky temperature models and their

influence on buildings energy performance: A critical review," *Energy Build.*, vol. 183, pp. 607–625, 2019.

[33] A. Hamza, I. M. S. Taha, and I. M. Ismail, "Cooling of water flowing through a night sky radiator," *Sol. Energy*, vol. 55, no. 4, pp. 235–253, 1995.

[34] U. Eicker and A. Dalibard, "Photovoltaic-thermal collectors for night radiative cooling of buildings," *Sol. Energy*, vol. 85, no. 7, pp. 1322–1335, 2011.

[35] X. Xu, R. Niu, and G. Feng, "An Experimental and Analytical Study of a Radiative Cooling System with Flat Plate Collectors," *Procedia Eng.*, vol. 121, no. 0, pp. 1574–1581, 2015.

[36] T. Q. Péan, L. Gennari, B. W. Olesen, and O. B. Kazanci, "Nighttime radiative cooling potential of unglazed and PV / T solar collectors : parametric and experimental analyses," *Proc. 8th Mediterr. Congr. Heating, Vent. Air-conditioning (climamed 2015)*, 2015.

[37] M. Hu *et al.*, "Experimental study on a hybrid photo-thermal and radiative cooling collector using black acrylic paint as the panel coating," *Renew. Energy*, vol. 139, pp. 1217–1226, 2019.

[38] M. Hu, B. Zhao, X. Ao, P. Zhao, Y. Su, and G. Pei, "Field investigation of a hybrid photovoltaic-photothermic-radiative cooling system," *Appl. Energy*, vol. 231, no. August, pp. 288–300, 2018.

[39] K. Zhang, D. Zhao, X. Yin, R. Yang, and G. Tan, "Energy saving and economic analysis of a new hybrid radiative cooling system for single-family houses in the USA," *Appl. Energy*, vol. 224, no. May, pp. 371–381, 2018.

[40] B. Zhao *et al.*, "A novel strategy for a building-integrated diurnal photovoltaic and all-day radiative cooling system," *Energy*, vol. 183, pp. 892–900, 2019.

[41] A. Aili *et al.*, "A kW-scale, 24-hour continuously operational, radiative sky cooling system: Experimental demonstration and predictive modeling," *Energy Convers. Manag.*, vol. 186, no. March, pp. 586–596, 2019.

[42] J. Liu *et al.*, "Research on the performance of radiative cooling and solar heating coupling module to direct control indoor temperature," *Energy Convers. Manag.*, vol. 205, no. December 2019, p. 112395, 2020.

[43] S. Vall and A. Castell, "Radiative cooling as low-grade energy source: A literature review," *Renew. Sustain. Energy Rev.*, vol. 77, no. May, pp. 803–820, 2017.

[44] M. Zeyghami, D. Y. Goswami, and E. Stefanakos, "A review of clear sky radiative cooling developments and applications in renewable power systems and passive building cooling," *Sol. Energy Mater. Sol. Cells*, vol. 178, no. August 2017, pp. 115–128, 2018.

[45] B. Zhao, M. Hu, X. Ao, N. Chen, and G. Pei, "Radiative cooling: A review of fundamentals, materials, applications, and prospects," *Appl. Energy*, vol. 236, no. November 2018, pp. 489–513, 2019.

[46] D. Singh, "Performance Analysis of Night Sky Radiant Cooling System (Nocturnal Radiator)," vol. 8, no. 1, pp. 2069–2078, 2018.

[47] "http://estacionmeteo.us.gter.es/." .

[48] "Weather station school of engineering university of Seville." .

[49] "https://www.ni.com/es-mx/shop/labview.html." .

[50] W. A. B. John A. Duffie, “Solar Engineering of Thermal Processes (third ed.), Wiley, New Jersey (2006).”

[51] F. P. Incropera, “Fundamentos de Transferencia de Calor.”

[52] “Geankoplis, C.J. Transport processes and separation process principles (2003). Fourth Edition, p. 475.”

[53] E. L. S. Mollons, “Manual técnico Solapool,” pp. 1–26.

[54] D. Pearlmutter and P. Berliner, “Experiments with a ‘psychrometric’ roof pond system for passive cooling in hot-arid regions,” *Energy Build.*, vol. 144, pp. 295–302, 2017.